Absorption and Emission Spectra and Structure Data of Single Crystal Maleonitriledithiolate Complexes of Platinum(II)

WOLFGANG GÜNTNER, GÜNTER GLIEMANN*
Institut für Physikalische und Theoretische Chemie, Universität Regensburg, D-8400 Regensburg (F.R.G.)
ULRICH KLEMENT and MANFRED ZABEL
Institut für Anorganische Chemie, Universität Regensburg, D-8400 Regensburg (F.R.G.)
(Received February 21, 1989)

Abstract

$[Bu_4N]_2[Pt(mnt)_2]$ crystallizes according to the space group $P\bar{1}$ with $Z = 1$. The anion $[Pt(mnt)_2]^{2-}$ is closely planar and has a center of symmetry at the platinum atom. The absorption spectra of single crystal $X_2[Pt(mnt)_2]$ exhibit a strong structured band at $\bar{\nu} \approx 20\,000$ cm^{-1} ($\epsilon \approx 3500$ l mol^{-1} cm^{-1}) and at its low-energy flank a system of weak bands with $\epsilon \approx 80$ l mol^{-1} cm^{-1}, which can be assigned to spin-allowed and spin-forbidden electronic transitions in the anion, respectively. The emission bands correspond to deactivations of the lowest excited triplet. The energies of the absorption and emission bands depend on the cation X.

Introduction

Transition metal dithiolene complexes exhibit several unusual properties such as strongly delocalized electronic structures, high stability, and a peculiar behavior of the one-electron oxidation–reduction [1–6]. For an understanding of these properties the knowledge of the molecular structure and of the character of the low-energy electronic states of the compounds is required. The purpose of this paper is to report such informations for the compound bis-(maleonitriledithiolate)platinum(II) $[Pt(mnt)_2]^{2-}$ with mnt $\equiv [S_2C_2(CN)_2]^{2-}$. For the tetra-n-butylammonium salt both the results of a X-ray structure analysis and the crystal morphology will be presented. The optical spectra of $[M(mnt)_2]^{2-}$ complexes with M = Ni, Pd, Pt published in the past have been recorded at $T \gtrsim 80$ K [7]. To understand more details of the electronic structure of the compounds it is appropriate to investigate the optical absorption and emission at a very low temperature. In this paper we report the low temperature absorption and emission spectra of single crystal $X_2[Pt(mnt)_2]$. Varying the counterion X^+ as

$[(Cetyl)Me_3N]^+ \equiv [CH_3(CH_2)_{15}N(CH_3)_3]^+$
$[Bu_4N]^+ \equiv [(C_4H_9)_4N]^+$
$[Et_4N]^+ \equiv [(C_2H_5)_4N]^+$
$[Ph_4P]^+ \equiv [(C_6H_5)_4P]^+$
$[Ph_4As]^+ \equiv [(C_6H_5)_4As]^+$
$[Me_4N]^+ \equiv [(CH_3)_4N]^+$
K^+

shows the influence of the counterion on the spectroscopic behavior of the complex in the solid state.

Experimental

The complexes were prepared following the method given in ref. 8 with the corresponding salts of the cations. For $K_2[Pt(mnt)_2]\cdot 2H_2O$ the potassium salt of the ligand was used. Crystals of good quality for X-ray structure analysis and spectroscopic investigations were obtained by slow evaporation from acetonitrile solutions in a refrigerator. The absorption and emission spectra were recorded with apparatus described in refs. 9–11. The structure of $[Bu_4N]_2[Pt(mnt)_2]$ was determined from a single crystal ($0.12 \times 0.12 \times 0.08$ mm) using Mo radiation and a graphite monochromator (Nonius CAD-4).

Results and Discussion

Structure

The elementary cell of single crystal $[Bu_4N]_2[Pt(mnt)_2]$ (at 24 °C) was calculated from 25 reflexes: $a = 9.855(2)$, $b = 10.838(3)$, $c = 12.346(2)$ Å, $\alpha = 85.52(2)$, $\beta = 87.89(1)$, $\gamma = 65.02(1)$. The space group is $P\bar{1}$ with $Z = 1$. A total of 4841 reflexes was

*Author to whom correspondence should be addressed.

0020-1693/89/$3.50

TABLE 1. Positional coordinates and isotropic thermal parameters for non-hydrogen atoms

Atom	x	y	z	B(Å^2)
Pt	0.0000	0.0000	0.0000	3.70(1)
S1	0.1551(2)	0.9597(2)	0.1449(2)	4.95(6)
S2	0.1133(7)	0.7740(2)	0.9682(2)	5.39(6)
N1	−0.2208(8)	−0.1323(7)	−0.3670(7)	7.2(2)
N2	−0.107(1)	0.4643(9)	0.2253(9)	9.8(3)
N3	−0.2914(6)	0.9141(5)	0.2772(5)	4.2(2)
C1	0.0904(7)	0.1198(7)	0.1943(7)	4.3(2)
C2	0.0227(7)	−0.2317(7)	−0.1462(7)	4.6(2)
C3	0.1590(8)	0.1284(8)	0.2900(8)	5.4(2)
C4	−0.0687(9)	0.3588(9)	0.1903(9)	6.9(2)
C5	−0.1313(7)	0.8077(7)	0.2566(7)	4.3(2)
C6	−0.0601(8)	0.7078(7)	0.3506(7)	5.0(2)
C7	0.1038(9)	0.6204(8)	0.3230(8)	6.3(2)
C8	0.178(1)	0.500(1)	0.409(1)	8.3(3)
C9	−0.3412(7)	1.0017(7)	0.1722(7)	4.7(2)
C10	−0.4959(9)	1.1167(9)	0.1755(9)	7.0(2)
C11	−0.466(1)	0.796(1)	−0.073(1)	8.7(3)
C12	−0.312(1)	0.671(1)	−0.074(1)	8.2(3)
C13	−0.3969(8)	0.8484(7)	0.3121(7)	5.0(2)
C14	−0.4186(7)	0.7647(7)	0.2281(7)	4.8(2)
C15	−0.4962(8)	0.6759(8)	0.2786(8)	6.0(2)
C16	0.4766(9)	−0.4079(9)	0.1949(9)	6.9(2)
C17	−0.2929(8)	1.0007(7)	0.3715(7)	5.0(2)
C18	−0.1830(9)	1.0648(9)	0.3575(8)	6.4(2)
C19	−0.212(1)	1.170(1)	0.447(1)	7.9(3)
C20	−0.355(1)	1.297(1)	0.427(1)	9.7(3)

measured using an $\omega/2\theta$-scan of $1.0 + 0.34 \times \text{tg}\ \theta$ width. The maximum scanning time was 60 s. The number of reflexes with an intensity greater than $3\sigma(I)$ was 4231. All reflexes were reduced to 2584 unique reflexes ($R_{\text{int}} = 0.025$).

The position of the Pt was taken from a Patterson synthesis. All other atoms, including hydrogen, were found from difference Fourier syntheses. The program DIFABS was used for absorption correction ($\mu = 31.8\ \text{cm}^{-1}$).

Isotropic refinement (193 variables) gave a R_w of 0.056. Anisotropic refinement (anion only, 223 variables) resulted in $R = 0.090$, $R_w = 0.049$, $w = 4I/(\sigma^2(I) + 0.002I^2)$. The positional and thermal parameters of all atoms are presented in Table 1.

The structure of $[Bu_4N]_2[Pt(mnt)_2]$ is isomorphous with the structures of the corresponding Co^{2+} and Ni^{2+} compounds [12, 13]. The molecular geometry of the $[Pt(mnt)_2]^{2-}$ anion is shown in Fig. 1, a projection onto the *ac* plane of the overall structure is illustrated in Fig. 2. The anion is almost planar and has a center of symmetry at the platinum atom. The equation of the plane, defined by the atoms Pt, C(1) and C(2), together with the distances of various atoms from this plane are given in Table 2. The interatomic bond lengths and angles are listed in Table 3. The anions are stacked along the *a* axis with the shortest Pt–Pt distance of the lattice constant. In

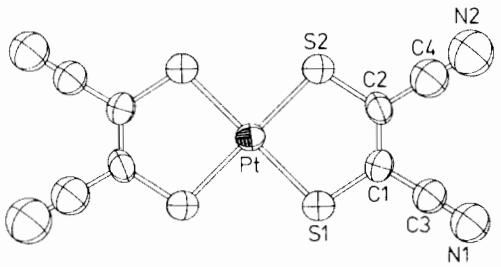

Fig. 1. Molecular geometry of the $[Pt(mnt)_2]^{2-}$ anion.

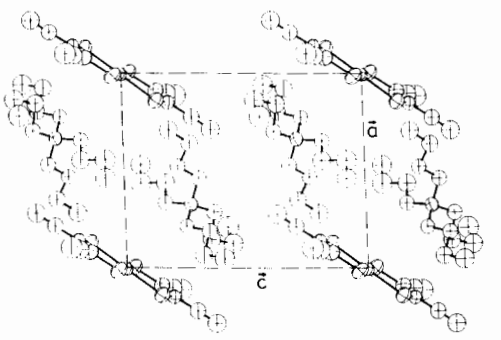

Fig. 2. Projection of the structure of $[Bu_4N]_2[Pt(mnt)_2]$ onto the *ac* plane.

TABLE 2. Least-squares plane for $[Pt(mnt)_2]^{2-}$ [a]

Atom	Deviation from the plane (Å)
Pt	0.000
C1	0.000(8)
C2	0.000(8)
S1	0.037(2)
S2	0.036(2)
C3	−0.063(9)
C4	−0.02(1)
N1	0.078(8)
N2	−0.02(1)

[a]Plane equation: $Ax + By + Cz - D = 0$ where x, y and z are orthogonalized coordinates. $A = 0.7969$, $B = 0.1403$, $C = -0.5876$, $D = 0.0$.

TABLE 3. Bond distances (Å) and angles (°) of $[Bu_4N]_2[Pt(mnt)_2]$

Bond distances		Bond angles	
$[Pt(mnt)_2]^{2-}$			
Pt–S1	2.287(2)	S1–Pt–S1	180.0
Pt–S2	2.279(2)	S1–Pt–S2	89.91(7)
S1–C1	1.727(8)	S1–Pt–S2	90.09(7)
S2–C2	1.715(9)	S1–Pt–S2	90.09(7)
N1–C3	1.16(2)	S1–Pt–S2	89.91(7)
N2–C4	1.15(2)	S2–Pt–S2	180.0
		Pt–S1–C1	101.8(3)
		Pt–S2–C2	102.2(3)
C1–C2	1.36(2)	S1–C1–C2	122.7(7)
C1–C3	1.41(1)	S1–C1–C3	116.1(6)
C2–C4	1.40(1)	C2–C1–C3	121.1(7)
		S2–C2–C1	123.0(6)
		S2–C2–C4	117.3(7)
		C1–C2–C4	119.7(8)
		N1–C3–C1	177.3(9)
		N2–C4–C2	180.0(1)
$[Bu_4N]^+$			
N3–C5	1.54(1)	C5–N3–C9	105.9(5)
N3–C9	1.51(2)	C5–N3–C13	112.4(6)
N3–C13	1.522(9)	C5–N3–C17	110.3(6)
N3–C17	1.54(2)	C9–N3–C13	111.6(6)
		C9–N3–C17	111.1(6)
		C13–N3–C17	105.8(5)
C5–C6	1.49(1)	N3–C5–C6	115.1(6)
C6–C7	1.53(1)	C5–C6–C7	109.1(8)
C7–C8	1.55(1)	C6–C7–C8	111.9(8)
C9–C10	1.51(1)	N3–C9–C10	114.8(7)
C11–C12	1.55(1)	N3–C13–C14	114.5(7)
C13–C14	1.51(1)	C13–C14–C15	110.9(8)
C14–C15	1.55(1)	C14–C15–C16	112.1(8)
C15–C16	1.53(1)	N3–C17–C18	114.1(7)
C17–C18	1.51(1)	C17–C18–C19	110.2(8)
C18–C19	1.58(1)	C18–C19–C20	112.0(2)
C19–C20	1.50(2)		

Table 3 the interatomic distances and angles of the $[Bu_4N]^+$ cation are given. Three of the butyl chains adopt the *trans* conformation, but one (with C(17)–C(20)) adopts the *gauche* conformation. That is unlike $[Bu_2N]_2[Cu(mnt)_2]$, in which two of the butyl chains exhibit *trans* and the other two *gauche* conformations, leading to a slightly shorter metal–metal separation [14] than in the Pt^{2+}, Co^{2+} and Ni^{2+} compounds. By optical goniometry measurements, along with the knowledge of the cell constants, the crystal faces could be identified to be of the form {100}, {010}, {001}, {110} and {101}, as shown in Fig. 3.

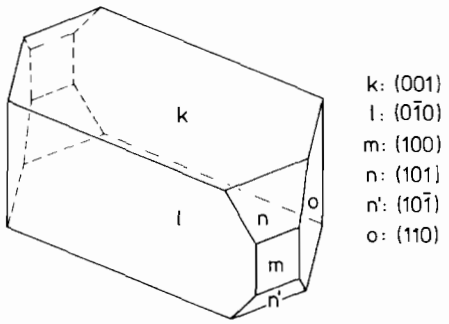

Fig. 3. Crystal morphology of $[Bu_4N]_2[Pt(mnt)_2]$.

Absorption and Emission Spectra

Figure 4 shows the absorption spectra of single crystals of $X_2[Pt(mnt)_2]$ at $T = 10$ K with X = [(Cetyl)Me_3N]$^+$ (a), $[Bu_4N]^+$ (b), $[Et_4N]^+$ (c), $[Ph_4P]^+$ (d), $[Ph_4As]^+$ (e), $[Me_4N]^+$ (f). The crystals had a thickness of about 1–2 μm; with $K_2[Pt(mnt)_2]\cdot 2H_2O$ (g) it was not possible to prepare such thin crystals. The low-temperature absorption spectra (except spectrum f) of the crystals are split into four peaks, which are more or less resolved, and show some shoulders at their blue flanks. The energetic distances of these four peaks are independent of the counterion of the complex. The strong absorption bands of $[Me_4N]_2[Pt(mnt)_2]$ are distinctly blue shifted in comparison with those of the other compounds. For $X_2[Pt(mnt)_2]$ dissolved in acetonitrile the extinction coefficient ϵ of the strong absorption bands in the visible region has values of about 3500 l mol^{-1} cm^{-1} [15].

Absorption measurements of thicker crystals (~100 μm) exhibit further weak bands with $\epsilon \sim 80$ l mol^{-1} cm^{-1} at the low-energy side of the strong absorption, as shown at the right hand side of Fig. 5. At $T \sim 10$ K all these weak band systems have a quite similar shape. They are well structured with a progression of about 1300 cm^{-1}. Their energy position depends distinctly on the counterion of the complex. The weak absorption bands of single crystal $[Me_4N]_2[Pt(mnt)_2]$ (f) and $K_2[Pt(mnt)_2]\cdot 2H_2O$ (g) have

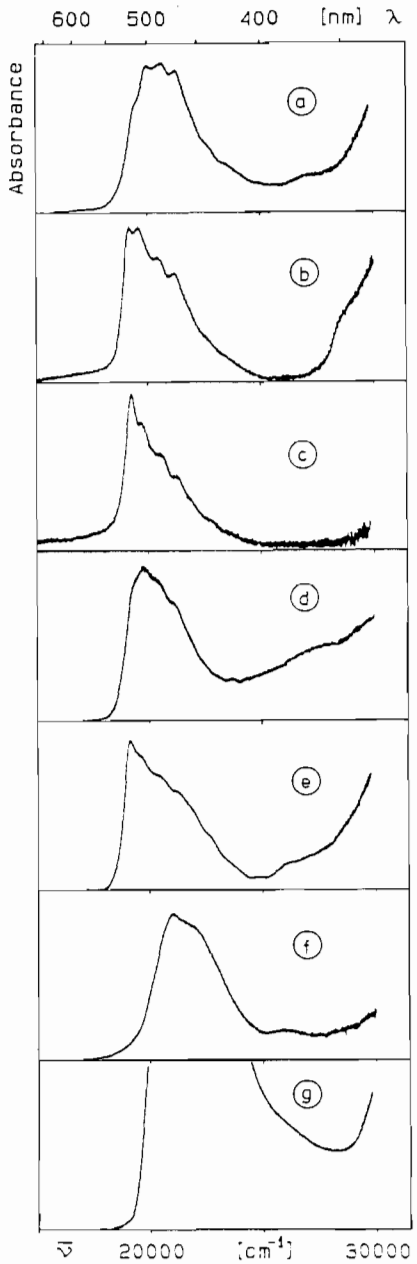

Fig. 4. Absorption spectra of single crystal $X_2[Pt(mnt)_2]$ complexes with different cations X^+ at $T = 10$ K.

significantly higher energies than the corresponding bands of the other compounds.

The left hand side of Fig. 5 shows the emission spectra at $T = 2$ K. The inserts represent the high-energy flanks of the emission bands recorded with high resolution on a larger scale. Each emission spectrum consists of a sharp line (spectra b, d, e f) or a shoulder (spectra a, c, g) at the blue side of the emission, followed by a broad band system at lower energies. On the whole these band systems of the different compounds have a similar shape, however, they differ by the form of the superimposed fine structure. The emission spectrum of $[Bu_4N]_2[Pt(mnt)_2]$ (b) at $T = 2$ K exhibits a particularly pronounced fine structure. For each compound the emission line (resp. shoulder) of highest energy overlaps with the red flank of the weak absorption of lowest energy.

The absorption spectrum of the $[Et_4N]_2[Pt(mnt)_2]$ complex in a KBr disc at room temperature and at $T = 80$ K has been reported by Clark and Turtle [7]. This spectrum agrees essentially with the strong 10 K absorption of the crystal in the visible, shown in Fig. 4, however, the fine structure is distinctly more pronounced at low temperature. Because of the large value of ϵ, the asymmetry of the band shape, and the occurrence of two maxima in the excitation profile of the corresponding Raman bands, they assigned this strong absorption to two electric-dipole allowed electronic transitions, a LMCT and a MLCT transition at $\bar{\nu} \sim 19\,153$ and $\bar{\nu} \sim 21\,181$ cm^{-1}, respectively. The remaining maxima and shoulders are caused by coupling of the electronic transitions with total-symmetric fundamentals (see Table 4). However, since all single crystals of $X_2[Pt(mnt)_2]$ described above and also the $[Et_4N]_2[Pd(mnt)_2]$ compound [7] exhibit very similar structured strong absorption bands, an assignment of the 21 181 cm^{-1} peak to an additional vibronic peak (with the $\bar{\nu}$(C≡N) fundamental) seems more likely.

TABLE 4. Raman active total symmetric fundamentals of $[Pt(mnt)_2]^{2-}$ [7]

Wavenumber (cm^{-1})	Assignment[a]
173.6	n.a.
377.6	ν(M–S)
495.5	n.a.
1007, 1043, 1057	ν(C–C) + ν(C–S)
1479	ν(C=C)
2194, 2222	ν(C≡N)

[a] n.a. = not assigned.

The system of weak bands at the low-energy side of the absorption spectrum (cf. right hand side of Fig. 5) can be assigned to the electronic transition to the lowest triplet state coupled with vibronic transitions of the ν(M–S) and ν(C=C) fundamentals.

The emission spectra can be explained in terms of a purely electronic (zero-phonon) transition from the lowest triplet state, yielding the sharp high-energy line in the spectra (see the inserts at the left hand side of Fig. 5), and a broad multi-phonon band at lower energy. This is a well known feature, already described in the literature for color centers in alkali

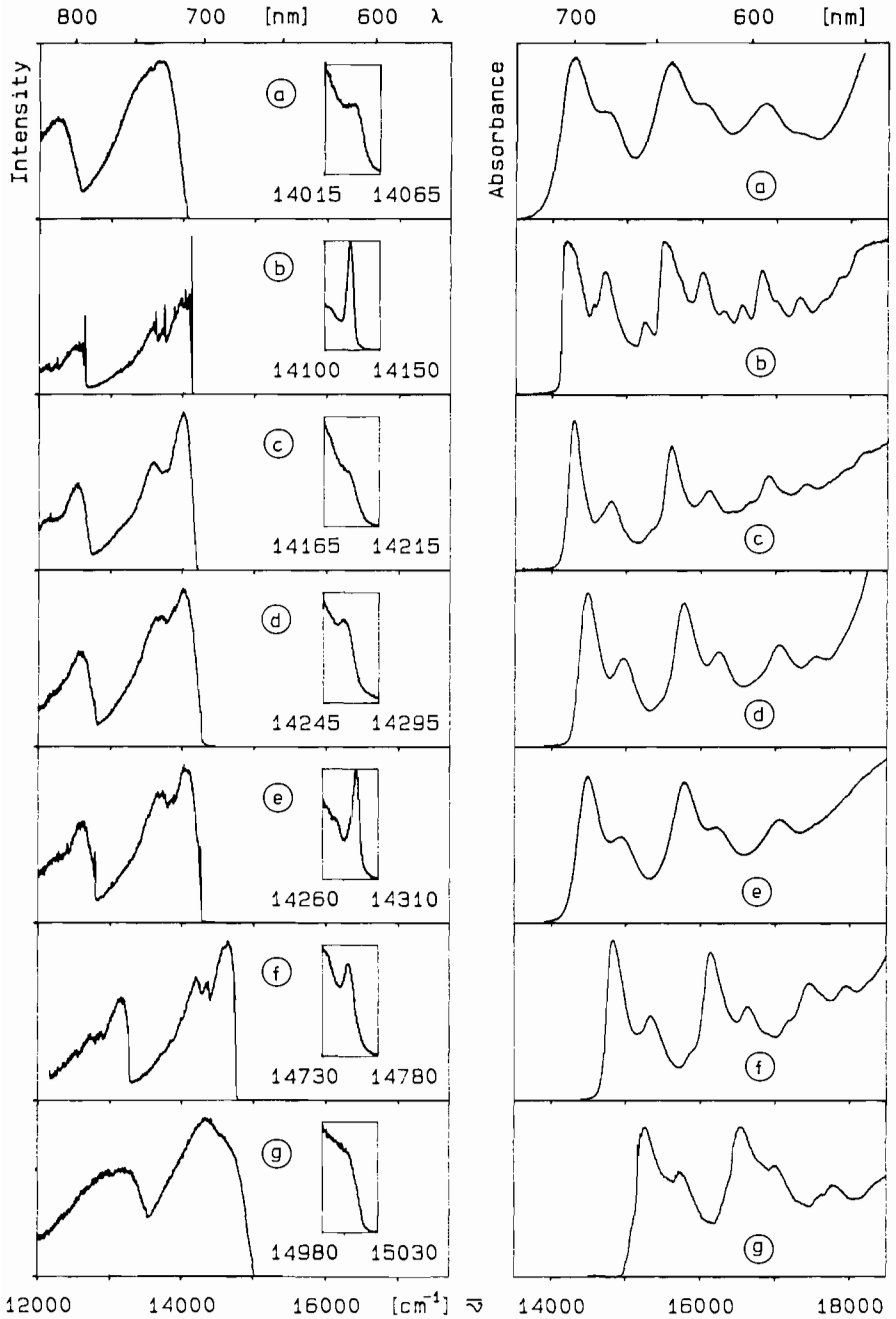

Fig. 5. Emission spectra (left hand side) and absorption spectra (right hand side) of single crystal $X_2[Pt(mnt)_2]$ complexes with different cations X^+ at $T = 2$ K (emission) and $T = 10$ K (absorption).

halides [16], for crystalline organic CT complexes [17] and transition metal complexes [18]. The relatively weak emission band, about 1500 cm^{-1} lower in energy than the most intense band, can be traced back from the latter by subtraction of a vibration quantum $\bar{\nu}$(C=C).

More information on the emission behavior of the $X_2[Pt(mnt)_2]$ complexes yields the low-temperature emission spectrum of single crystal $[Bu_4N]_2[Pt(mnt)_2]$ which exhibits a pronounced fine structure superimposed on the multi-phonon band, cf. left hand side of Fig. 5b. The sharp lines appearing in addition to the high-energy zero-phonon line can be assigned to vibrational satellites of the latter, due to total-symmetric vibrational modes as mentioned in Table 4. The emission spectra of the crystalline $[Pt(mnt)_2]^{2-}$ complexes with other counterions show no corresponding fine structure lines or only weakly

pronounced ones. This may be caused by different strengths of the electron–phonon coupling in the different crystals.

The energy of the zero-phonon transition can be tuned over about 1000 cm^{-1} by varying the counterion, cf. the inserts at the left hand side of Fig. 5. That the type of cation can influence the optical transition energies of solid transition metal compounds is well known, an example are the crystalline tetracyanoplatinates(II) [19]. Their absorption and emission energies depend strongly on the intercomplex coupling and, therefore, on the minimum Pt–Pt distance, which is in the order of ~3–4 Å. This distance, however, is determined by the type of cation (and by the crystal water content). For single crystals $X_2[Pt(mnt)_2]$ this explanation fails, since the minimum Pt–Pt distance in these crystals is relative large (9.855 Å for $X^+ = [Bu_4N]^+$), indicating that the intercomplex Pt–Pt coupling is negligible and, therefore, it cannot influence the absorption and emission energies. The dependence of these energies on the cation is rather due to a direct interaction between the $[Pt(mnt)_2]^{2-}$ complex ions and the cations, as suggested recently for solids of the similar compounds $[Bu_4N]_2[Ni(mnt)_2]$ and $[Me_4N]_2[Ni(mnt)_2]$ [20]. Depending on the size and the site of the cation it can effect the π-electron system of the complex anion. The $[Me_4N]^+$ cation will exert a weaker coupling than the larger $[Bu_4N]^+$ cation, yielding for single crystal $[Me_4N]_2[Ni(mnt)_2]$ a higher absorption energy than for the tetra-n-butylammonium complex. The same trend holds true for the corresponding Pt(II) complexes. Crystals with small cations have higher optical transition energies than with larger ones.

Further investigations concerning the dependence of the polarized absorption and emission of single crystal $X_2[Pt(mnt)_2]$ on external magnet fields and on temperature are in progress.

Acknowledgement

We wish to acknowledge the support of Fonds der Chemischen Industrie.

References

1 J. A. McCleverty, *Prog. Inorg. Chem., 10* (1968) 49.
2 R. Eisenberg, *Prog. Inorg. Chem., 12* (1970) 295.
3 J. S. Miller and A. J. Epstein, *Prog. Inorg. Chem., 20* (1976) 1.
4 R. P. Burns and C. A. McAuliffe, *Adv. Inorg. Chem. Radiochem., 22* (1978) 303.
5 L. Alcácer and H. Novais, in J. S. Miller (ed.), *Extended Linear Chain Compounds,* Vol. 3, Plenum, New York, 1983, Ch. 6.
6 S. Alvarez, R. Vicente and R. Hoffmann, *J. Am. Chem. Soc., 107* (1985) 6253.
7 R. J. H. Clark and P. C. Turtle, *J. Chem. Soc., Dalton Trans.,* (1977) 2142.
8 A. Davison and R. Holm, *Inorg. Synth., 10* (1967) 8.
9 W. Tuszynski and G. Gliemann, *Ber. Bunsenges. Phys. Chem., 89* (1985) 940.
10 H. Yersin and G. Gliemann, *Messtechnik, 80* (1972) 99.
11 G. Gliemann, *Comments Inorg. Chem., 5* (1986) 263.
12 J. D. Forrester, A. Zalkin and D. H. Templeton, *Inorg. Chem., 3* (1964) 1500.
13 A. Kobayashi and Y. Sasaki, *Bull. Chem. Soc. Jpn., 50* (1977) 2650.
14 K. W. Plumlee, B. M. Hoffmann, J. A. Ibers and Z. G. Soos, *J. Chem. Phys., 63* (1975) 1926.
15 S. I. Shupack, E. Billig, R. J. H. Clark, R. Williams and H. B. Gray, *J. Am. Chem. Soc., 86* (1964) 4594.
16 D. B. Fitchen, R. H. Silsbee, T. A. Fulton and E. L. Wolf, *Phys. Rev. Lett., 11* (1963) 275.
17 D. Haarer, *J. Chem. Phys., 67* (1977) 4076.
18 E. Gallhuber, G. Hensler and H. Yersin, *Chem. Phys. Lett., 120* (1985) 445.
19 G. Gliemann and H. Yersin, *Struct. Bonding (Berlin), 62* (1985) 87.
20 S. Lalitha, G. V. R. Chandramouli and P. T. Manoharan *Inorg. Chem., 27* (1988) 1492.